A R C H I V E S O F M E T A L L U R G Y A N D M A T E R I A L S
Volume 58 2013 Issue 2
DOI: 10.2478/amm-2013-0006

R. GAWEL*, M. VIVIANI**, K. PRZYBYLSKI*

LONG-TERM CHEMICAL STABILITY OF $BaCe_{0,85}Y_{0,15}O_{3-\delta}$ + $Ce_{0,85}Y_{0,15}O_{2-\delta}$ COMPOSITE SAMPLES AT ROOM TEMPERATURE AND AT 873 K FOR USE IN DUAL PCFC-SOFC FUEL CELLS

DŁUGOCZASOWA STABILNOŚĆ PRÓBEK KOMPOZYTOWYCH $BaCe_{0,85}Y_{0,15}O_{3-\delta}$ + $Ce_{0,85}Y_{0,15}O_{2-\delta}$ W TEMPERATURZE POKOJOWEJ ORAZ 873 K DO ZASTOSOWANIA W OGNIWACH PALIWOWYCH TYPU PCFC-SOFC

The goal of this work is to compare the long-term chemical stability of $BaCe_{0,85}Y_{0,15}O_{3-\delta}$ and $Ce_{0,85}Y_{0,15}O_{2-\delta}$ bulk composite samples to that of pure $BaCe_{0,85}Y_{0,15}O_{3-\delta}$ after ageing for 600 hours in CO_2/H_2O atmosphere at room temperature and N_2/H_2O atmosphere at 873 K. Differential Thermal Analysis and Thermogravimetry were used to investigate the physicochemical processes that took place during the ageing of the afore-mentioned samples and the chemical composition of the gases released from the samples was analyzed by a Mass Spectrometer. The influence of the reactive atmospheres on phase and chemical composition, as well as the microstructure of the bulk samples, was determined from X-ray Diffraction results and Scanning Electron Microscopy observations combined with Energy Dispersion Spectroscopy analysis. From these studies it can be concluded that the composite materials are capable of maintaining stability in the studied conditions, however, pure $BaCe_{0,85}Y_{0,15}O_{3-\delta}$ is unstable in CO_2/H_2O atmosphere at room temperature.

Keywords: perovskites, solid oxide fuel cell electrolytes, chemical stability, composite materials

Celem pracy jest porównanie długoczasowej stabilności chemicznej spieków kompozytowych $BaCe_{0,85}Y_{0,15}O_{3-\delta}$ i $Ce_{0,85}Y_{0,15}O_{2-\delta}$ z czystym $BaCe_{0,85}Y_{0,15}O_{3-\delta}$, które poddano starzeniu przez 600 godzin w atmosferze CO_2/H_2O w temperaturze pokojowej oraz w atmosferze N_2/H_2O w 873 K. Do badań procesów fizykochemicznych zachodzących podczas starzenia w/w próbek wykorzystano metodę termicznej analizy różnicowej oraz termograwimetrię, natomiast skład chemiczny gazów uwalnianych z próbek podczas ich ogrzewania analizowano spektrometrem masowym. Wpływ atmosfer reakcyjnych na skład fazowy i chemiczny oraz mikrostrukturę spieków określono w oparciu o wyniki badań rentgenograficznych oraz obserwacji przy pomocy skaningowej mikroskopii elektronowej połączonej z dyspersją energii promieniowania rentgenowskiego. Z badań tych można wnioskować, że materiały kompozytowe wykazują stabilność w badanych warunkach, podczas gdy czysty $BaCe_{0,85}Y_{0,15}O_{3-\delta}$ jest nietrwały w atmosferze CO_2/H_2O w temperaturze pokojowej.

1. Introduction

Solid oxide fuel cells (SOFCs) have been considered as promising materials for motorization, combined heat and power systems, as well as auxiliary power units, due to their relatively high efficiency (50-60%) amongst fuel cells, clean chemical to electrical energy conversion, reliability, modularity, fuel adaptability and quiet, vibration-free operation. For many years such fuel cells have been based on Yttria-stabilized Zirconia (YSZ) as the electrolyte material, which conducts oxide ions in the temperature range 1073-1273 K, as determined by Nernst in 1899 [1]. Unfortunately, such high operating temperatures lead to high material degradation rates and limit the possible interconnect materials. Therefore, ceramic materials capable of oxide ion conduction at lower temperatures were investigated. One of these materials was cerium dioxide, also known as ceria (CeO_2). It was found that ceria possesses oxygen vacancies ($V_O^{\bullet\bullet}$) as the predominant ionic defect [2], due to which the material becomes an oxygen deficient n-type semiconductor at elevated temperatures. Later the influence of yttria (Y_2O_3) on the ceria defect structure was investigated [3-5]. From these studies it was determined that the number of oxygen vacancies, and subsequently, the oxide ion conductivity of ceria increases with Y_2O_3 concentration. The Kroger-Vink notation [6] describing the effect of Y_2O_3 on the oxygen vacancy concentration is shown in Eq. (1) [7]:

$$Y_2O_3 \xrightarrow{CeO_2} 2Y'_{Ce} + 3O_O^x + V_O^{\bullet\bullet} \tag{1}$$

Eventually, yttria-doped ceria (YDC) was considered as an electrolyte material for intermediate temperature solid oxide fuel cells (IT-SOFCs) [8], i.e., SOFCs capable of operating in the intermediate temperature range (873-1073 K).

In 1981, Iwahara et al. discovered that materials based on $SrCeO_3$ were capable of conducting protons in hydrogen atmosphere at elevated temperatures [9]. Since then, similar

* AGH UNIVERSITY OF SCIENCE AND TECHNOLOGY, 30-059 KRAKÓW, POLAND
** INSTITUTE FOR ENERGETICS AND INTERPHASES, NATIONAL RESEARCH COUNCIL, GENOA, ITALY

perovskite based materials, such as $BaCeO_3$, $CaZrO_3$, $BaZrO_3$ and $SrZrO_3$, in which cerium or zirconium is substituted by trivalent cations (Y^{3+}, Gd^{3+}, Sc^{3+}, Nd^{3+} or In^{3+}), have been investigated as proton conducting materials [10-12]. Among various competitors, it was determined that $BaCeO_3$ doped with Y^{3+} (BCY) exhibits the highest proton conductivity at intermediate temperatures [13-16]. It was also found that 15% of the dopant corresponds to the maximum conductivity at 873 K [17]. However, $BaCeO_3$ based materials have the tendency to decompose in the presence of atmospheres containing CO_2 and/or H_2O, according to Eq. (2) and Eq. (3) [18,19]:

$$BaCeO_3 + CO_2 \rightarrow BaCO_3 + CeO_2 \quad (2)$$

$$BaCeO_3 + H_2O \rightarrow Ba(OH)_2 + CeO_2 \quad (3)$$

Therefore, several attempts have been made to improve the chemical stability of BCY via the substitution of cerium by Zr [20,21] or Ti [22,23] cations. While the presence of Zr and Ti cation dopants increased the chemical stability of the material [20-23], they also lowered its conductivity [21,23].

Modern IT-SOFCs and PCFCs are both capable of operating in the temperature range 873-973 K, which opens new possibilities concerning interconnect materials and metal supported fuel cell designs. Still, a fundamental disadvantage remains in all SOFCs and PCFCs: the production of water during the electrochemical half-reaction that takes place at the anode side of the fuel cell in the case of SOFCs and at the cathode side in the case of PCFCs, which, in both cases, leads to low fuel and electrical efficiency, interconnect corrosion and necessity for a gas counter-flow. In order to eliminate this flaw, the concept of a dual PCFC-SOFC, which operates in the temperature range 873-973 K was introduced [24]. The idea behind this new type of fuel cell is to connect a PCFC anode compartment (anode/electrolyte) with a SOFC cathode compartment (electrolyte/cathode) through a porous central membrane material capable of both proton and oxide-ion conductivity. In the central membrane, protons formed at the anode react with oxide anions formed at the cathode, which creates water that is evacuated through the porous membrane, as shown in Fig. 1.

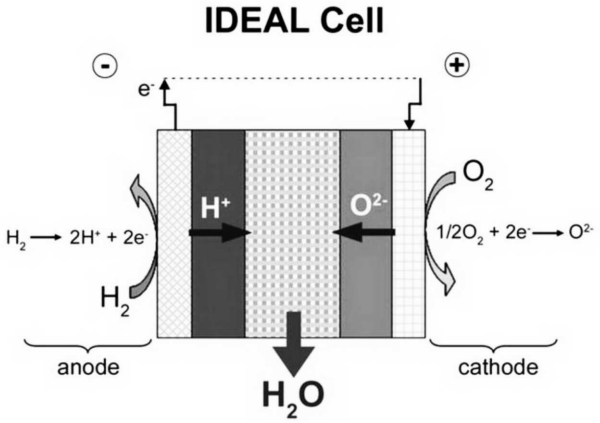

Fig. 1. Schematic representation of the dual PCFC-SOFC fuel cell concept [24]

Potential materials for such application are composites consisting of $BaCe_{0.85}Y_{0.15}O_{3-\delta}$ (BCY15) mixed together with $Ce_{0.85}Y_{0.15}O_{2-\delta}$ (YDC15) in different molar ratios. BCY15 and YDC15 are compatible materials [25] since the latter is a decomposition product of the first one at high temperature (1723 K) when BCY15 is Ba deficient [24]. Furthermore, it is assumed that YDC15, i.e., CeO_2 doped with 15% Y_2O_3, will affect the equilibrium of Eq. (2) and Eq. (3) according to the Le Chatelier-Braun principle and thereby increase the stability of BCY15. The goal of this work is to compare the chemical stability of BCY15-YDC15 bulk samples in the presence of water vapour at 873 K, as well as a mixture of CO_2 and H_2O at room temperature, with that of pure BCY15.

2. Experimental procedure

In order to prepare the BCY15-YDC15 composite samples, BCY15 and YDC15 powders were synthesized via oxalate co-precipitation using barium, cerium and yttrium dissolved salts. Composite powders, the approximate compositions of which are given in TABLE 1, were then obtained via 24 hr. ball milling (120-150 rpm) of the two powders in a PET bottle (vol 100 ml) in presence of Zr- balls (4 balls with diameter=15 mm, 34 balls with diameter=10 mm, 98 g of balls with diameter=5 mm) by adding isopropanol (≈20 ml). Afterwards, the mixtures were freeze dried (the bottles were frozen in liquid nitrogen) and finally the mixtures were separated from Zr-balls by sieving (53μm mesh).

TABLE 1
Designation and approximate composition of each sample

Designation	Composition [% mol]
BCY15	$BaCe_{0.85}Y_{0.15}O_{3-\delta}$
B90Y10	90% $BaCe_{0,85}Y_{0,15}O_{3-\delta}$+ 10% $Ce_{0,85}Y_{0,15}O_{2-\delta}$
B70Y30	70% $BaCe_{0,85}Y_{0,15}O_{3-\delta}$+ 30% $Ce_{0,85}Y_{0,15}O_{2-\delta}$
Y70B30	30% $BaCe_{0,85}Y_{0,15}O_{3-\delta}$+ 70% $Ce_{0,85}Y_{0,15}O_{2-\delta}$
Y80B20	20% $BaCe_{0,85}Y_{0,15}O_{3-\delta}$+ 80% $Ce_{0,85}Y_{0,15}O_{2-\delta}$
Y90B10	10% $BaCe_{0,85}Y_{0,15}O_{3-\delta}$+ 90% $Ce_{0,85}Y_{0,15}O_{2-\delta}$

Each of the obtained powders was annealed at 1373 K for 2 $^1/_2$ hrs (heating/cooling rate: 10 K/min) in flowing synthetic air and then pressed under 25MPa into 2 pellets with 5 mm diameters and 2 mm thicknesses. Afterwards, the pellets were heated with a rate of 2.5 K/min, sintered at 1473 K in flowing synthetic air for 2 hrs. and cooled at 5 K/min. One bulk sample of each compound was exposed to CO_2/H_2O rich atmosphere in a vacuum desiccator for 600 hrs and the powders and other bulk samples were entered into an experimental setup shown in Fig. 2. In this system, N_2 was supplied to a saturator for 600 hrs at a flow rate of 50cm^3/min, as determined by the mass flow controller. The saturator was surrounded by a heating element, which ensured a water temperature of 353 K, allowing the nitrogen to capture a relatively high percentage of water vapour (46,8 %mol.) before entering the reaction tube. In the reaction tube, quartz crucibles containing the bulk samples were placed in the isothermal zone of the furnace, where 873 K was maintained, and the samples were exposed to the N_2/H_2O mixture.

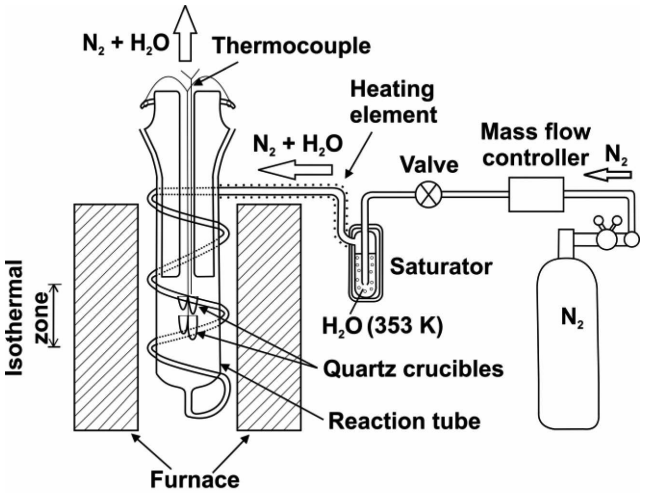

Fig. 2. Scheme of the experimental setup used to expose the samples to N_2/H_2O atmosphere

Differential Thermal Analysis (DTA), Thermogravimetry (TG) and Mass Spectrometry (MS) were carried out for the samples using a microthermogravimetric apparatus (SDT-2960 by TAInstruments, USA) coupled with a quadruple gas analyzer (Thermostar GSD 300 by Balzers, Liechtenstein). During the DTA-TG-MS analysis, the samples were heated up to 1473 K continuously with a rate of 20 K/min in a stream of flowing synthetic air with a rate of 100cm^3/min and the mass changes of the samples were registered continuously with simultaneous gas analysis in the direct vicinity of the sample.

Analysis of the microstructure and chemical composition of the powders and bulk samples was provided using Scanning Electron Microscopy combined with Energy Dispersive Spectroscopy (SEM-EDS). The phase composition of the samples was determined by X-ray Diffraction (XRD).

3. Results

SEM microphotographs of the initial BCY15 and YDC15 powders before mixing are presented in Fig. 3. From Fig. 3a it follows that BCY15 powder grains are round and non-agglomerated. Their size ranges between 80 and around 400 nm. On the other hand, large aggregates are visible in the YDC15 powder (Fig. 3b), the size of which ranges between 0.5 and 2.0 μm.

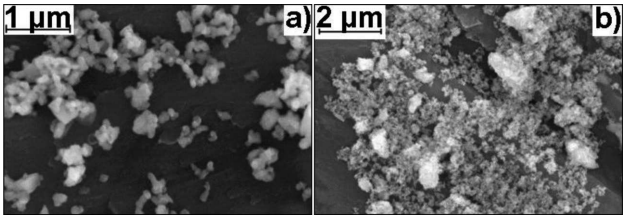

Fig. 3. SEM microphotographs of initial: a) $BaCe_{0.85}Y_{0.15}O_{3-\delta}$ (BCY15) and b) $Ce_{0.85}Y_{0.15}O_{2-\delta}$ (YDC15) powders

The mass changes of the bulk samples during heating combined with DTA and MS analysis after saturation in CO_2/H_2O rich atmosphere for 600 hrs at room temperature are presented in Fig. 4. From the TG curves, one step of mass loss up to 473 K is observed as a result of H_2O detachment from the composite samples as confirmed by MS analysis. MS studies of the composites also show very minor effects associated with desorption of CO_2 from the samples. From this it can be concluded that the adsorption of CO_2 at room temperature and subsequent formation of $BaCO_3$ inside the composite samples in CO_2/H_2O atmosphere at room temperature is negligible. However, in the case of BCY15 two definite steps of mass loss can be easily distinguished: up to 473 K as a result of H_2O desorption and beyond 973 K due to the decomposition of $BaCO_3$. Furthermore, the mass loss resulting from H_2O desorption in the case of BCY15 is the largest, whereas the lowest mass loss is seen for Y90B10.

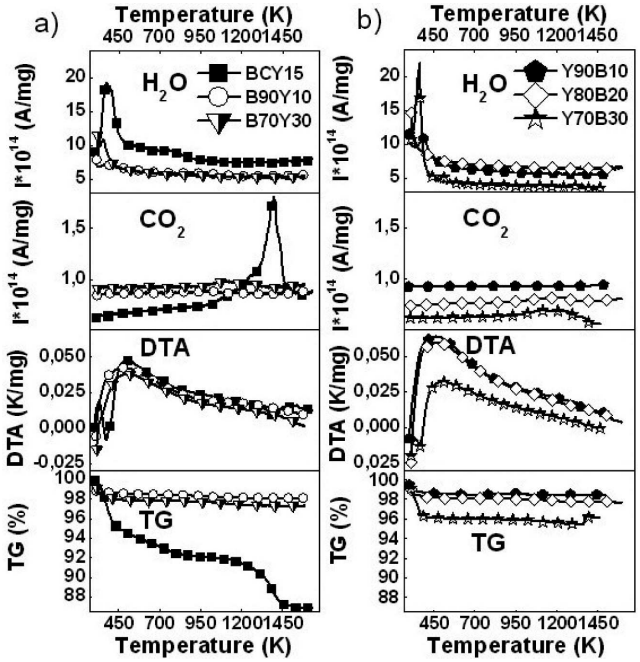

Fig. 4. MS, DTA and TG curves of: a) BCY15, B90Y10 and B70Y30 and b) Y90B10, Y80B20 and Y70B30 bulk samples after ageing in CO_2/H_2O rich atmosphere at room temperature for 600 hrs

TABLE 2 shows the calculated approximate values of the mass fractions of $BaCO_3$ and H_2O in each bulk sample after exposure to CO_2/H_2O for 600 hrs at room temperature. From these results it follows that the amount of $BaCO_3$ determined in the case of BCY15 is very significant compared to the amounts in the composite samples, which do not exceed 2%wt. It is also confirmed that BCY15 captured a larger amount of water than the composite materials. Among the composites, the largest combined amount of CO_2 and H_2O was adsorbed by Y70B30 and the lowest amount by Y90B10.

The mass changes of the powders during heating combined with MS analysis after exposure to N_2/H_2O rich atmosphere at 873 K are shown in Fig. 5. From these combined MS-TG studies it follows that mass loss from desorption of H_2O from composite samples is not observed. In the case of the BCY15 powder, MS analysis confirms changes in the amounts of CO_2 and H_2O at temperatures below 973 K resulting from desorption of these compounds from the surface of the powder. For each of the powders, the TG analysis confirms that total mass loss does not exceed 1%wt. and the MS studies indicate that the mass loss of the powders beyond 973 K is due to the decomposition of small amounts of $BaCO_3$ present

in the materials due to manipulation of the samples in air. The cause of the very small mass changes at temperatures below 973 K is unknown and will be the subject of further research. It is possible these mass changes are the result of oxygen diffusing into and from the powders. However, the use of flowing synthetic air (~21 %vol. O_2) would make such small changes in the oxygen signal practically invisible in the MS analysis and therefore the theory remains pure speculation.

TABLE 2

Mass fractions of $BaCO_3$ and H_2O in the bulk samples after the effects of CO_2/H_2O atmosphere at room temperature for 600 hrs as determined from the MS-DTA-TG analysis presented in Fig. 4

Composition	%wt. $BaCO_3$	%wt. H_2O
$BaCe_{0,85}Y_{0,15}O_{3-\delta}$	23.3	7.8
$0,9BaCe_{0,85}Y_{0,15}O_{3-\delta}$ + $0,1Ce_{0,85}Y_{0,15}O_{2-\delta}$	1.3	1.5
$0,7BaCe_{0,85}Y_{0,15}O_{3-\delta}$ + $0,3Ce_{0,85}Y_{0,15}O_{2-\delta}$	1.8	2.2
$0,3BaCe_{0,85}Y_{0,15}O_{3-\delta}$ + $0,7Ce_{0,85}Y_{0,15}O_{2-\delta}$	1.8	4.0
$0,2BaCe_{0,85}Y_{0,15}O_{3-\delta}$ + $0,8Ce_{0,85}Y_{0,15}O_{2-\delta}$	1.3	1.9
$0,1BaCe_{0,85}Y_{0,15}O_{3-\delta}$ + $0,9Ce_{0,85}Y_{0,15}O_{2-\delta}$	0.4	1.4

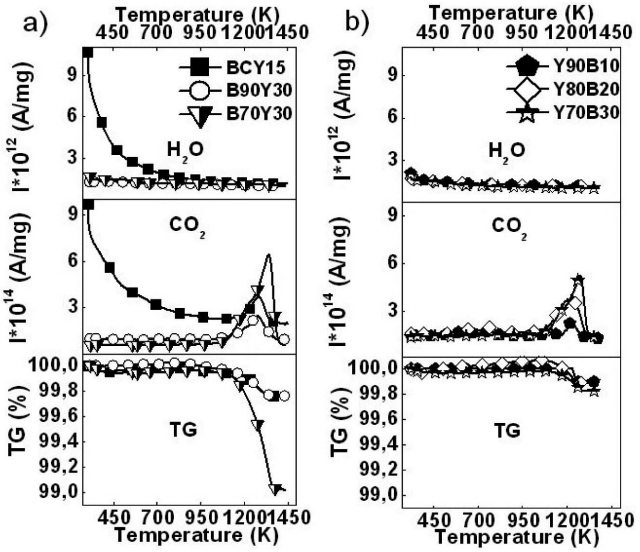

Fig. 5. MS and TG curves of: a) BCY15, B90Y10 and B70Y30 and b) Y90B10, Y80B20 and Y70B30 powders after ageing in N_2/H_2O rich atmosphere at 873°C for 600 hrs

TG studies combined with DTA after saturation in N_2/H_2O rich atmosphere at 873 K are presented in Fig. 6. In this figure, the TG courses also show minor mass losses (below 0.25 %wt.) in the case of each sample. The largest mass loss is observed in the case of the B90Y10 bulk sample and the lowest mass loss is seen in the case of Y80B20. The mass loss for bulk samples beyond 973 K is similar to that observed in Fig. 5 and it can therefore also be contributed to the decomposition of baseline amounts of $BaCO_3$. As in the case of the powders, the cause of the very minor mass changes at temperatures below 973 K has not yet been determined and will be the subject of further research. In this case, the mass loss can also be explained as oxygen, captured by the material during prolonged exposure to N_2/H_2O atmosphere, now diffusing from the bulk samples. Unfortunately, this is also not determined.

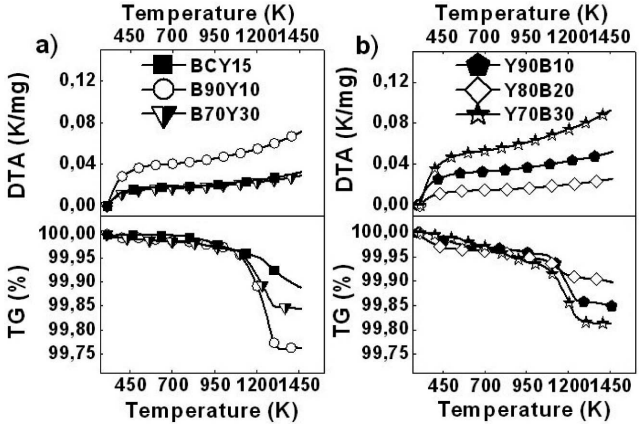

Fig. 6. DTA and TG curves of: a) BCY15, B90Y10 and B70Y30 and b) Y90B10, Y80B20 and Y70B30 bulk samples after ageing in N_2/H_2O rich atmosphere at 873 K for 600 hrs

SEM analysis of BCY15 after saturation in CO_2/H_2O rich atmosphere at room temperature and after exposure to N_2/H_2O rich atmosphere is shown in Fig. 7. The fractures in Fig. 7a confirm that BCY15 was unable to maintain cohesion after the combined effects of CO_2 and H_2O at room temperature. In turn, no micro-fractures are visible in Fig. 7b, from which it can be concluded that the corrosive effects of N_2/H_2O atmosphere on BCY15 are negligible at 873 K.

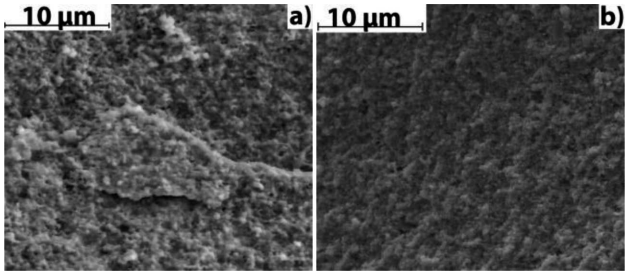

Fig. 7. SEM images of BCY15 bulk sample after a) exposure to CO_2/H_2O atmosphere at room temperature and b) exposure to N_2/H_2O atmosphere at 873 K

The presence of $BaCO_3$ in BCY15 after saturation in CO_2/H_2O atmosphere at room temperature was confirmed via XRD analysis. In all other cases, additional phases were not detected. As an example, Fig. 8 and Fig. 9 show XRD analysis of Y70B30 after the effects of CO_2/H_2O (Fig. 8) and N_2/H_2O (Fig. 9). In Fig. 8, $BaCO_3$ was not detected due to the small amount of the compound in the sample. Moreover, the baseline/signal ratio of the XRD studies was high, because the analysis was carried out on a small piece of a sample with an uneven surface. Unfortunately, this means that peak(s) corresponding to the presence of $BaCO_3$ in the sample are most likely hidden in the background.

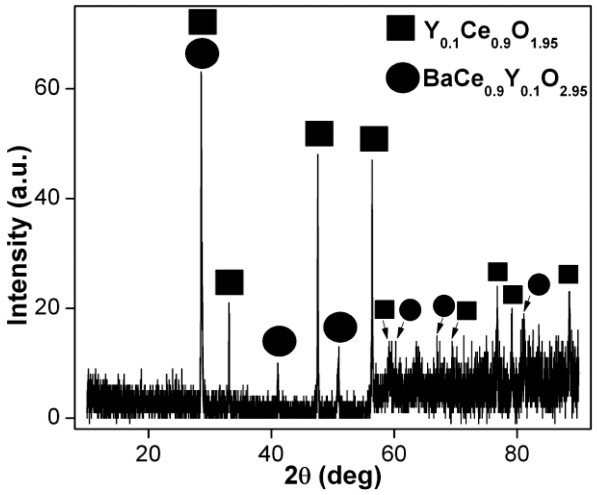

Fig. 8. XRD analysis of Y70B30 bulk sample after exposure to CO_2/H_2O rich atmosphere at room temperature

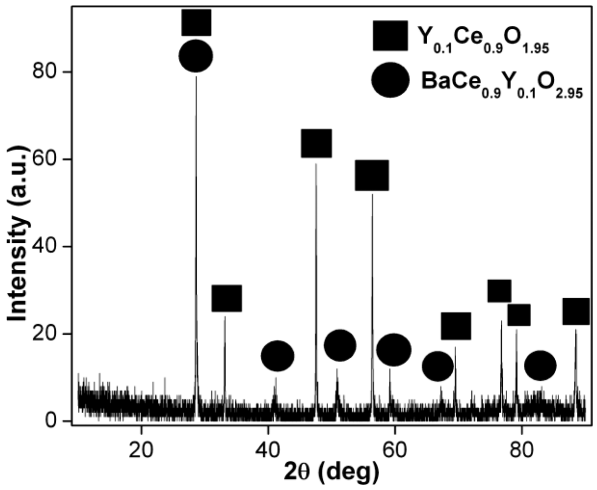

Fig. 9. XRD analysis of Y70B30 bulk sample after exposure to N_2/H_2O rich atmosphere at 873 K

4. Conclusions

The corrosive effects of water vapour at 873 K on both BCY15 and the composite samples are practically nonexistent, whereas at room temperature the effects of H_2O have been determined. Furthermore, the addition of YDC15 in the composite materials significantly improves the resistance of BCY15 against both water vapour and CO_2. As a result, all composite materials exhibit long-term stability in atmospheres containing CO_2 and H_2O at normal temperatures and are capable of maintaining cohesion in dual PCFC-SOFC fuel cell operating conditions. From this it can be concluded that BCY15-YDC15 composite materials meet the necessary chemical stability requirements for potential use as dual PCFC-SOFC central membrane materials.

Acknowledgements

The research leading to these results has received funding from the European Union's Seventh Framework Programme (FP7/2007-2013) under grant agreement No 213389. The authors are also grateful to Dr. Eng. Ryszard Gajerski for his assistance with the DTA-TG-MS analysis, Dr. Eng. Anna Adamczyk for the XRD analysis and Dr. Eng. Barbara Trybalska for her assistance with the SEM-EDS analysis.

REFERENCES

[1] W. Nernst, Z. Elektrochem. **6**, 41 (1899).
[2] B.C.H. Steele, J.M. Floyd, Proc. Br. Ceram. Soc. **19**, 55 (1971).
[3] M.P. Anderson, D.E. Cox, K. Halperin, A.S. Nowick, Solid State Ionics. **9-10**, 953 (1983).
[4] D.Y. Wang, A.S. Nowick, J. Phys. and Chem. Solids. **44**, 639 (1983).
[5] K. Fuda, K. Kishio, S. Yamauchi, K. Fueki, J. Phys. and Chem. Solids **46**, 1141 (1985).
[6] F.A. Kröger, H.J. Vink, Solid State Phys. **3**, 307 (1956).
[7] M. Hartmanova, E.E. Lomonova, V. Navratil, P. Sutta, F. Kundracik, J. Mater. Sci. **40**, 5679 (2005).
[8] N.Q. Minh, J. Am. Ceram. Soc. **76**, 563 (1993).
[9] H. Iwahara, T. Esaka, H. Uchida, N. Maeda, Solid State Ionics. **3-4**, 359 (1981).
[10] H. Iwahara, H. Uchida, K. Ono, K. Ogaki, J. Electrochem. Soc. **135**, 529 (1988).
[11] T. Yajima, H. Kazeoka, T. Yogo, H. Iwahara, Solid State Ionics. **47**, 271 (1991).
[12] H. Iwahara, T. Yajima, T. Hibino, K. Ozaki, H. Suzuki, Solid State Ionics. **61**, 65 (1993).
[13] T. Hibino, A. Hashimoto, M. Suzuki, M. Sano, J. Electrochem. Soc. **149**, A1503 (2002).
[14] T. Shimura, H. Tanaka, H. Matsumoto, T. Yogo, Solid State Ionics. **176**, 2945 (2005).
[15] W. Suksamai, I.S. Metcalfe, Solid State Ionics. **178**, 627 (2007).
[16] X.Z. Fu, J.L. Luo, A.R. Sanger, N. Luo, K.T. Chuang, J. Power Sources. **195**, 2659 (2010).
[17] G. Chiodelli, L. Malavasi, C. Tealdi, S. Barison, M. Battagliarin, L. Doubova, M. Fabrizio, C. Mortalo, R. Gerbasi, J. Alloy Compd. **470**, 477 (2009).
[18] S. Gopalan, A.V. Virkar, J. Electrochem. Soc. **140**, 1060 (1993).
[19] C.W. Tanner, A.V. Virkar, J. Electrochem. Soc. **143**, 1386 (1996).
[20] K. Katahira, Y. Kohchi, T. Shimura, H. Iwahara, Solid State Ionics. **138**, 91 (2000).
[21] P. Sawant, S. Varma, B.N. Wani, S.R. Bharadwaj, Int. J. Hydrogen Energy. **37**, 3848 (2012).
[22] P. Pasierb, E. Drożdż-Cieśla, R. Gajerski, S. Łabuś, S. Komornicki, M. Rękas, J. Therm. Anal. Calor. **96**, 475 (2009).
[23] K. Xie, R. Yan, X. Liu, J. Alloys Comp. **479**, L40 (2009).
[24] A.S. Thorel, M. Chesnaud, M. Viviani, A. Barbucci, S. Presto, P. Piccardo, Z. Ilhan, D. Vladikova, Z. Stoynov, ECS Trans. **25**, 753 (2009).
[25] G. Caboche, J.-F. Hochepied, P. Piccardo, K. Przybylski, R. Ruckdäschel, M.-R. Ardigó, E. Fatome, S. Chevalier, A. Perron, L. Combemale, M. Palard, J. Prażuch, T. Brylewski, ECS Trans. **25**, 763 (2009).

Received: 20 January 2013.